

Imaging Mechanical Vibrations in Suspended Graphene Sheets

D. Garcia-Sanchez,^{†,‡} A. M. van der Zande,[§] A. San Paulo,[‡] B. Lassagne,^{†,‡}
P. L. McEuen,[§] and A. Bachtold^{*,†,‡}

CIN2 Barcelona, Campus UAB, E-08193 Bellaterra, Spain, CNM-CSIC Barcelona,
Campus UAB, E-08193 Bellaterra, Spain, and Cornell Center for Materials Research,
Cornell University, Ithaca, New York 14853

Received January 21, 2008; Revised Manuscript Received March 27, 2008

ABSTRACT

We carried out measurements on nanoelectromechanical systems based on multilayer graphene sheets suspended over trenches in silicon oxide. The motion of the suspended sheets was electrostatically driven at resonance using applied radio frequency voltages. The mechanical vibrations were detected using a novel form of scanning probe microscopy, which allowed identification and spatial imaging of the shape of the mechanical eigenmodes. In as many as half the resonators measured, we observed a new class of exotic nanoscale vibration eigenmodes not predicted by the elastic beam theory, where the amplitude of vibration is maximum at the free edges. By modeling the suspended sheets with the finite element method, these edge eigenmodes are shown to be the result of nonuniform stress with remarkably large magnitudes (up to 1.5 GPa). This nonuniform stress, which arises from the way graphene is prepared by pressing or rubbing bulk graphite against another surface, should be taken into account in future studies on electronic and mechanical properties of graphene.

Graphene is a newly isolated material whose structure consists of a single layer of carbon atoms packed in a honeycomb crystal lattice.^{1,2} Recently, stacks of graphene layers were suspended over a trench and clamped at the edges, obtaining a new type of nanoelectromechanical system (NEMS).³ Despite thicknesses all the way down to one atomic layer, these suspended stacks of graphene still maintain high crystalline order,⁴ resulting in a NEMS with extraordinarily small thickness, large surface area, low mass density, and high Young's modulus. Because of these excellent material properties, graphene NEMSs hold promise as very good detectors of mass, force, and charge and represent the ultimate limit of two-dimensional NEMSs.

Previous work has shown suspended graphene sheets can be mechanically actuated, and the resonant frequencies are extracted using optical interferometry. However, this measurement technique can not identify what the individual vibrational eigenmodes are.³ In this work, we directly image the spatial shape of the eigenmodes using a scanning force microscope (SFM). While the eigenmode shape can match predictions for doubly clamped beams typically discussed in elastic beam theory text books, we also observe new exotic eigenmodes in as many as half the suspended sheets measured. These exotic eigenmodes would be impossible to identify using more traditional measurement techniques, such

as optical or capacitive detection, which depend on the average position of the resonator.^{3,5}

Few-layer suspended graphene sheets were obtained by mechanical exfoliation.^{6,7} Highly ordered bulk graphite was pressed down onto a degenerately doped silicon wafer patterned with trenches etched into the oxide and with gold electrodes defined between the trenches. Suitable candidates for measurement were identified optically,^{8,9} looking for few-layer graphene sheets suspended over a trench and contacting at least one electrode. A scanning electron microscope image of a suspended graphene sheet used in these experiments is shown in Figure 1a.

The suspended graphene sheets were electrostatically actuated to become resonators by wiring them up as shown in Figure 1b. An oscillating radio frequency voltage V_{RF} was applied between the back gate and the graphene, resulting in an oscillating electrostatic force at the same frequency:

$$F_{\text{RF}} = \frac{\partial C}{\partial z} (V_{\text{DC}} - \varphi) V_{\text{RF}} \quad (1)$$

where V_{DC} is the dc voltage applied to the gate, φ is the contact potential between the resonator and the gate, and $\partial C/\partial z$ is the spatial derivative of the capacitance between the resonator and the gate.

The mechanical vibration of the resonator was detected using a recently reported SFM technique, which allowed the measurement of the resonance frequency as well as the shape of the eigenmode.¹⁰ This technique is particularly suitable for the detection of low amplitude vibrations, which

* Corresponding author. E-mail: adrian.bachtold@cnm.es.

[†] CIN2 Barcelona.

[‡] CNM-CSIC Barcelona.

[§] Cornell Center for Materials Research, Cornell University.

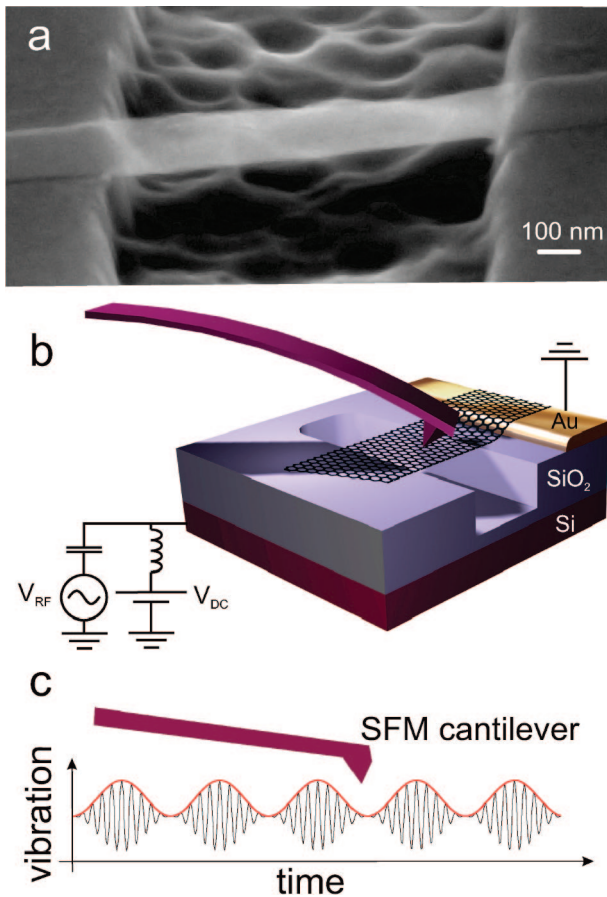


Figure 1. Device and experimental setup. (a) A scanning electron microscope image of a suspended graphene resonator. (b) Schematic of the resonator together with the SFM cantilever. (c) Motion of the suspended graphene sheet as a function of time. A high-frequency term at f_{RF} is matched to the resonance frequency of the graphene, and the resulting oscillation is modulated at f_{mod} .

here are typically of the order of 0.1 nm (see Supporting Information). As shown in Figure 1b, a SFM cantilever scans over the surface of the suspended sheet, while the resonator is being driven. The frequency f_{RF} of the driving voltage V_{RF} is set at (or close to) the resonance frequency of the resonator. In addition, V_{RF} is modulated at f_{mod} , $(1 - \cos(2\pi f_{mod}t)) \cos(2\pi f_{RF}t)$, so the resonator vibrations are sequentially turned on and off at f_{mod} (Figure 1c). While the SFM cantilever cannot follow the rapid oscillations at f_{RF} , it can detect the height difference between the on and off states of the modulation envelope. To enhance the detection sensitivity to the vibrations, f_{mod} is matched to the resonance frequency of the first eigenmode of the SFM cantilever. At the same time, the topography is obtained with the second eigenmode of the cantilever to keep the tip at a constant height above the surface. Further details on the technique can be found in Supporting Information.

Table 1 summarizes the dimensional characteristics of the suspended sheets that we have studied, such as the thickness t , length l , and width w , as well as the resonance frequencies. The measured quality factors are low (between 2 and 30). This low Q is attributed to energy dissipation to air molecules because the SFM technique is operated at atmospheric conditions.^{10,11} The shape of the eigenmodes does not change

Table 1. Resonator Characteristics^a

l (μm)	t (nm)	w (μm)		f_1 (MHz)	f_2 (MHz)	mode
		min	max			
2.9	1	0.1	0.8	18		beam
2.7	3	0.8	1.8	45		beam
4.4	6	0.5	0.8	33		beam
1.8	10	0.2	0.6	37		beam
2.8	11	0.3	0.5	31		beam
2.9	20	0.6	1.0	57		beam
4.2	4	1.3	1.5	25	59	edge
2.8	5	0.8	1.0	47		edge
3.5	6	1.0	1.4	33	70	edge
2.8	6	0.5	0.8	53	85	edge
2.9	10	0.7	1.5	26		edge

^a l is the length of the resonator, t the thickness, w the width, and f_1 (f_2) the resonance frequency of the first (second) eigenmode. w can significantly vary along the resonator, so we report the minimum and the maximum width.

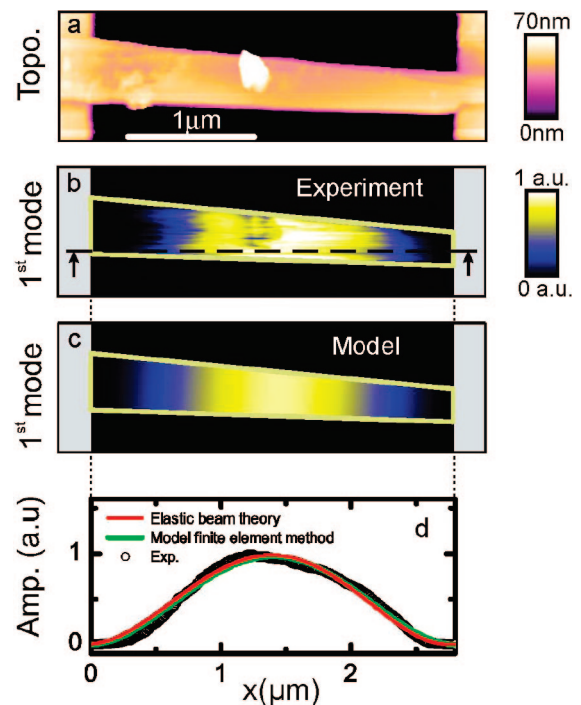


Figure 2. Graphene resonator with no buckling. (a) Measured topography. The image reveals irregularities on the surface of the resonator, presumably due to contamination or bulk graphite residue. $t = 11$ nm, $l = 2.8$ μm , $w_{\min} = 0.3$ μm , and $w_{\max} = 0.5$ μm . (b) Measured shape of the eigenmode at 31 MHz (raw data). $V_{DC} - \varphi = 3$ V and $V_{RF} = 60$ mV. The amplitude of vibration is in arbitrary units. (c) Shape of the eigenmode at 31 MHz obtained using FEM simulations without any stress. (d) Eigenmode along the line indicated in Figure 2b.

as the frequency is swept (within a same resonance peak of the amplitude versus frequency). All measurements are performed in the linear amplitude response regime. See Supporting Information for further details.

The SFM technique yields high resolution images of the shape of the vibration eigenmodes because the scanning SFM tip measures the amplitude of vibration as a function of position. We find two distinct types of eigenmodes in the suspended graphene resonators. Figures 2a and 3a show the height topography images of two different suspended graphene sheets with thicknesses of 11 and 6 nm, respectively. Figures

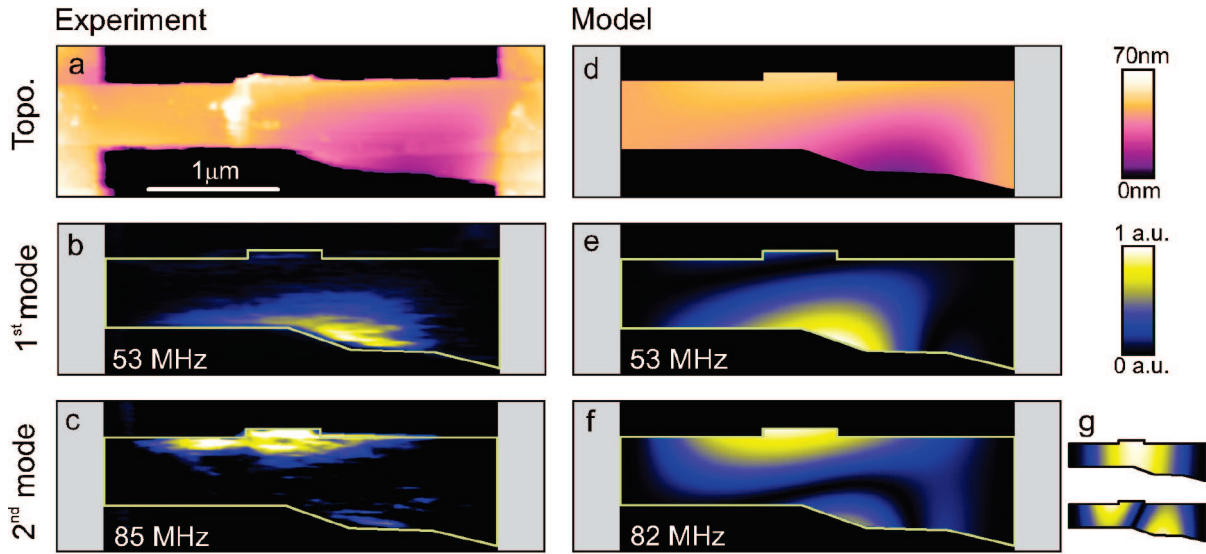


Figure 3. Graphene resonator with local buckling. (a) Measured topography. $t = 6$ nm, $l = 2.8$ μm , $w_{\text{min}} = 0.5$ μm , and $w_{\text{max}} = 0.8$ μm . The maximum out-of-plane displacement of the buckling is 37 nm. (b–c) Shape of the first and the second eigenmodes (raw data). $V_{\text{DC}} - \varphi = 3$ V and $V_{\text{RF}} = 40$ mV. The amplitude of vibration is in arbitrary units. (d) Topography obtained using FEM simulations on a stressed graphene sheet. The maximum displacement is 36 nm. See the text for the boundary conditions. (e–f) Shape of the first and the second eigenmodes using FEM simulations. (g) Shape of the two first eigenmodes using FEM simulations without any stress. The resonance frequencies are 17 and 46 MHz.

2b and 3b,c show the corresponding eigenmodes with respective resonance frequencies 31, 53, and 85 MHz, respectively. For some resonators, the amplitude of vibration remains uniform across the width of the sheet similar to standard beam resonators (Figure 2b), while for others, the vibrations are the largest in amplitude along one of the free edges (Figure 3b,c). We call the former modes “beam modes” and the latter “edge modes”.

Let us first compare the beam modes to predictions from the elastic beam theory, which describes the dynamics of a linear resonator with a uniform cross-section.¹² A beam under weak uniform tension T is predicted to have a fundamental mode resonance frequency of

$$f_1 = \frac{1.028}{l^2} \sqrt{\frac{Et^2}{\rho}} + T \frac{0.154}{\sqrt{\rho E w^2 t^4}} \quad (2)$$

where the shape of the first eigenmode along the beam axis x is predicted to be

$$z_1 = \left[\cos\left(\frac{4.73x}{l}\right) - \cosh\left(\frac{4.73x}{l}\right) \right] - 0.98 \left[\sin\left(\frac{4.73x}{l}\right) - \sinh\left(\frac{4.73x}{l}\right) \right] \quad (3)$$

where the Young’s Modulus is $E = 1$ TPa and the mass density is $\rho = 2200$ kg m^{-3} . Taking the values $l = 2.8$ μm and $t = 11$ nm for the graphene sheet shown in Figure 2 and assuming $T = 0$, eq 2 predicts a resonance frequency $f_1 = 31$ MHz, in excellent agreement with the experimentally measured value. In addition, we find that eq 3 qualitatively describes the measured eigenmode shape (as shown in Figure 2d). Note, however, that eqs 2 and 3 are calculated when the resonator is perpendicular to the clamping edge and has a constant width along the beam axis. The topography image of the suspended sheet shows that this is not the case (Figure 2a). We have developed a model based on the finite element method (FEM) to take these complications into account (see

Supporting Information). Parts c and d of Figure 2 show the predicted eigenmode shape of the resonator according to FEM. The predicted eigenmode has resonance frequency of 31 MHz, in excellent agreement with the measurements. The shape agrees qualitatively with the measurements and remains very similar to the predictions of the elastic beam theory.

Not all suspended graphene sheets display such conventional eigenmodes. The edge modes shown in Figure 3b,c are completely unpredicted by standard elastic beam theory. However, the topography image of the suspended sheet in Figure 3a shows that the resonator is buckled out of plane at one edge. This local buckling is measured to have a maximum out-of-plane displacement of 37 nm and suggests the presence of nonuniform stress in the resonator. The edge modes are frequently, but not always, observed in resonators for which the suspended sheet displays local buckling.

To understand the relationship between local buckling and the edge modes, we calculate the effect of strain with simulations based on the finite element method (see Supporting Information). The strain is introduced by imposing an in-plane stretch and in-plane rotation to the suspended sheet at the clamping edges. In Figure 3d, we impose an in-plane stretch of 1.5 nm and in-plane rotation of -0.2° about a pivot point at the top right of the resonator. This strain results in local buckling in the lower edge with a maximum out-of-plane displacement of 36 nm, consistent with measurement. Parts e and f of Figure 3 show the predicted eigenmodes for the buckled sheet. Both the resonance frequencies and shapes are in reasonable agreement with measurements. For comparison, simulations carried out without any stress result in conventional beam modes as shown in Figure 3g.

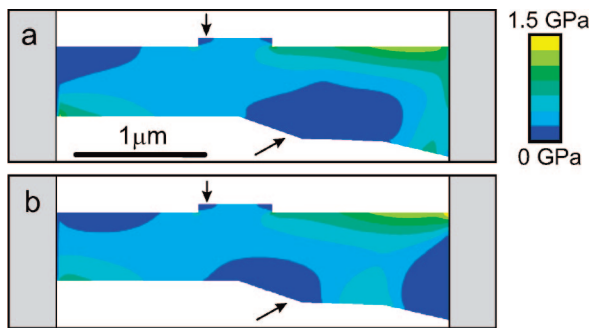


Figure 4. Calculated principal stress σ_1 for the suspended graphene sheet in Figure 3. The color scale shows the stress in the resonator, ranging from 0 to 1.5 GPa. (a) Top surface. (b) Bottom surface. Arrows indicate regions with low stress where the amplitude of the eigenmodes is maximum.

This good agreement overall allows us to use the simulation to evaluate the stress in the resonator. Stress is described by a 3×3 tensor that varies over the volume of the resonator:¹³

$$\sigma_{ij} = \begin{bmatrix} \sigma_x & \tau_{xy} & \tau_{xz} \\ \tau_{yx} & \sigma_y & \tau_{yz} \\ \tau_{zx} & \tau_{zy} & \sigma_z \end{bmatrix} \quad (4)$$

where σ_i is the stress along axis i and τ_{ij} is the shearing stress in plane ij . A suitable transformation of the direction of the coordinate axes through rotation allows the components of the shearing stress τ_{ij} to vanish. The result is a diagonal matrix with 3 components: σ_1 , σ_2 , and σ_3 , where $\sigma_1 > \sigma_2$, σ_3 , and σ_1 is known as the principal stress. Note that this transformation is made for each point of the resonator. The maximum value of the principle stress before a material breaks is used as the failure criteria for crystalline materials.¹³

Figure 4 shows the spatial distribution of σ_1 over the top and the bottom surfaces of the suspended sheet from Figure 3. In between these two boundary surfaces, σ_1 varies continuously (not shown). The maximum stress in the suspended sheet is very high, about 1.5 GPa. For comparison, it has been shown that 1020 steel breaks at 690 MPa,¹³ MWNTs between 11 and 63 GPa,¹⁴ and SWNTs between 13 and 52 GPa.¹⁵ We attribute this high stress to be the consequence of the macroscopic uncontrolled forces that are applied during the mechanical exfoliation process step. Part of the resulting stress remains after the applied forces are released due to the large van der Waals interaction that holds the graphene to the SiO₂ surface.

Comparing Figures 3 and 4, it appears that the distribution of stress and the resonance properties are closely related. The vibration amplitude is larger in regions of lower stress. In addition, there is a correlation between the resonance modes and regions of increasing stress: the fundamental eigenmode resonates at the lower free edge where the stress is the lowest, and the second eigenmode resonates at the upper edge where the stress is larger. The underlying physical mechanism is the same as for a beam under uniform tension for which the resonance frequency increases as the tension is raised.¹⁶

To conclude, we have imaged the eigenmode shape of graphene resonators. For some resonators, we have found a new class

of nanoscale eigenmodes where the vibrations are maximum in amplitude, not at the center of the beam but at the free edges. Simulations based on the finite element method indicate that these eigenmodes are the result of the high nonuniform stress present in the resonator. The shape of these exotic eigenmodes and the corresponding stress must be taken into account in future experiments and applications, such as for the determination of the Young's modulus^{17,18} and the accurate calibration of mass, force, or charge sensing.^{3,19,20} It could also be possible to manipulate the eigenmode shape by varying the strain during measurements via electrostatic tuning,³ varying the pressure difference across sealed membranes, or displacing the clamping edges. This would allow one to activate mechanical vibrations in localized areas for multiple-target sensing applications. It is also important to realize that stress can be present in graphene sheets regardless of whether they are suspended or not. This stress needs to be taken into account when engineering the band gap of graphene ribbons,^{21–23} in measuring the amplitude and wavelength of ripples,^{24,25} or in estimating the effective magnetic field in quantum electron interference experiments.^{26,27}

Acknowledgment. We thank Scott Verbridge and Jeevak Parpia for help with sample characterization. The research has been supported by a EURYI grant and FP6-IST-021285-2 and by the NSF through the Cornell Center for Materials Research. Sample fabrication was performed at the Cornell Nanoscale Science and Technology Facility, a National Nanotechnology Infrastructure Network node, funded by NSF.

Supporting Information Available: A detailed description of fabrication technique, a description of the FEM model, a comparison of the FEM model to analytical predictions for a beam under tension²⁸ as well as recent simulations on nanotubes with slack,²⁹ and a detailed description of the SFM technique to detect mechanical vibrations. This material is available free of charge via the Internet at <http://pubs.acs.org>.

References

- (1) Castro Neto, A.; Guinea, F.; Peres, N. M. *Phys. World* **2006**, *19*, 33.
- (2) Geim, A. K.; Novoselov, K. S. *Nat. Mater.* **2007**, *6*, 183.
- (3) Bunch, J. S.; van der Zande, A. M.; Verbridge, S. S.; Frank, I. W.; Tanenbaum, D. M.; Parpia, J. M.; Craighead, H. G.; McEuen, P. L. *Science* **2007**, *315*, 490.
- (4) Meyer, J. C.; Geim, A. K.; Katsnelson, M. I.; Novoselov, K. S.; Booth, T. J.; Roth, S. *Nature* **2007**, *446*, 60.
- (5) Sazonova, V.; Yaish, Y.; Üstünel, H.; Roundy, D.; Arias, T. A.; McEuen, P. L. *Nature* **2004**, *431*, 284.
- (6) Novoselov, K. S.; Geim, A. K.; Morozov, S. V.; Jiang, D.; Zhang, Y.; Dubonos, S. V.; Grigorieva, I. V.; Firsov, A. A. *Science* **2004**, *306*, 666.
- (7) Novoselov, K. S.; Jiang, D.; Schedin, F.; Booth, T. J.; Khotkevich, V. V.; Morozov, S. V.; Geim, A. K. *Proc. Natl. Acad. Sci. U.S.A.* **2005**, *102*, 10451.
- (8) Blake, P.; Hill, E. W.; Castro Neto, A. H.; Novoselov, K. S.; Jiang, D.; Yang, R.; Booth, T. J.; Geim, A. K. *Appl. Phys. Lett.* **2007**, *91*, 063124.
- (9) Abergel, D. S. L.; Russell, A.; Fal'ko, V. I. *Appl. Phys. Lett.* **2007**, *91*, 063125.
- (10) Garcia-Sanchez, D.; San Paulo, A.; Esplandiú, M. J.; Perez-Murano, F.; Forró, L.; Agüasca, A.; Bachtold, A. *Phys. Rev. Lett.* **2007**, *99*, 085501.
- (11) Ekinci, K. L.; Roukes, M. L. *Rev. Sci. Instrum.* **2005**, *76*, 061101.
- (12) Weaver, W.; Timoshenko, S. P.; Young, D. H. *Vibrations Problems in Engineering*. Wiley: New York, 1990.

- (13) Ford, H.; Alexander, J. M. *Advanced Mechanics of Materials*; Longmans: London, 1963.
- (14) Yu, M. F.; Lourie, O.; Dyer, M. J.; Moloni, K.; Kelly, T. F.; Ruoff, R. S. *Science* **2000**, *287*, 637.
- (15) Yu, M. F.; Files, B. S.; Arepalli, S.; Ruoff, R. S. *Phys. Rev. Lett.* **2000**, *84*, 5552.
- (16) Verbridge, S. S.; Shapiro, D. F.; Craighead, H. G.; Parpia, J. M. *Nano Lett.* **2007**, *7*, 1728.
- (17) Frank, I. W.; Tanenbaum, D. M.; van der Zande, A. M.; McEuen, P. L. *J. Vac. Sci. Technol., B* **2007**, *25*, 2558.
- (18) Poot, M.; van der Zant, H. S. J. *Appl. Phys. Lett.*, **2007**, *92*, 063111.
- (19) Craighead, H. *Nat. Nanotechnol.* **2007**, *2*, 18.
- (20) Tamayo, J.; Ramos, D.; Mertens, J.; Calleja, M. *Appl. Phys. Lett.* **2006**, *89*, 224104.
- (21) Fiori, G.; Iannaccone, G. *IEEE Electron Device Lett.* **2007**, *28*, 760.
- (22) Yang, L.; Anantram, M. P.; Han, J.; Lu, J. P. *Phys. Rev. B* **1999**, *60*, 13874.
- (23) Yang, L.; Han, J. *Phys. Rev. Lett.* **2000**, *85*, 154.
- (24) Fasolino, A.; Los, J. H.; Katsnelson, M. I. *Nat. Mater.* **2007**, *6*, 858.
- (25) Morozov, S. V.; Novoselov, K. S.; Katsnelson, M. I.; Schedin, F.; Elias, D. C.; Jaszczak, J. A.; Geim, A. K. *Phys. Rev. Lett.* **2008**, *100*, 016602.
- (26) Morozov, S. V.; Novoselov, K. S.; Katsnelson, M. I.; Schedin, F.; Ponomarenko, L. A.; Jiang, D.; Geim, A. K. *Phys. Rev. Lett.* **2006**, *97*, 016801.
- (27) Morpurgo, A. F.; Guinea, F. *Phys. Rev. Lett.* **2006**, *97*, 196804.
- (28) Buks, E.; Roukes, M. L. *Phys. Rev B* **2001**, *63*, 033402.
- (29) Üstünel, H.; Roundy, D.; Arias, T. A. *Nano Lett* **2005**, *5*, 523.

NL080201H